ELSEVIER

International Journal of Mass Spectrometry 185/186/187 (1999) 437–447

International Journal of Mass Spectrometry

# Dissociation of $N_2O^+$ ions from the valence states reached by one-photon photoionisation

E. Kinmond[a], J.H.D. Eland[a,*], L. Karlsson[b]

[a]*Physical and Theoretical Chemistry Laboratory, South Parks Road, Oxford OX1 3QZ, UK*
[b]*Physics Institute, Uppsala University, Box 530, S-751 21 Uppsala, Sweden*

Received 5 June 1998; accepted 8 September 1998

**Abstract**

The dissociation of $N_2O^+$ from the states reached by one-photon ionisation at 58.4 and 30.4 nm has been examined by photoelectron–photoion coincidence spectroscopy. At 30.4 nm, ions formed in some inner valence states dissociate rapidly enough to show a forward/backward asymmetry between the electron and fragment ion ejection directions. In the 19 to 20 eV energy region, the dissociation characteristics suggest the existence of an additional electronic state. The kinetic energy releases identify the final channels in dissociation from several states; the energy releases in $N_2^+$ formation from states in the inner valence region are consistent with known fluorescence emission from $N_2^+$ ($B\ ^2\Sigma_u^+$) fragments and suggest that emissions from $N_2^+$($A\ ^2\Pi_u$) may also be present. (Int J Mass Spectrom 185/186/187 (1999) 437–447) © 1999 Elsevier Science B.V.

*Keywords:* PEPICO; $N_2O^+$ dissociation; Kinetic energy release

## 1. Introduction

Nitrous oxide is a linear asymmetric molecule with the valence electronic configuration

$$(5\sigma)^2(6\sigma)^2(1\pi)^4(7\sigma)^2(2\pi)^4\ X\ ^1\Sigma^+$$

The outer valence ionic states, seen prominently in the HeI photoelectron spectrum [1–4] are X $^2\Pi$ (12.89 eV), A $^2\Sigma^+$ (16.38 eV), B $^2\Pi$ (17.65 eV), and C $^2\Sigma^+$ (20.11 eV). In the inner valence region from 20 to 40 eV, calculations [5,6] predict the existence of many states that could be populated by multiple electron transitions. The few photoelectron spectra covering the inner valence region [4,7,8] show only broadbands which overlap each other, with no vibrational structure at the resolution used. The only experimental identifications of inner valence bands come from e,2e spectroscopy [9,10], where six bands at energies below 40 eV were assigned as satellites of different main line (one-electron) transitions, in broad agreement with the theoretical predictions.

The dissociation of $N_2O^+$ has been investigated by photoionisation mass spectrometry [11,12], photoelectron–photoion coincidence (PEPICO) [13,14], threshold photoelectron–photoion coincidence (TPEPICO) [15–17], and also by fast ion beam laser (FIBLAS) experiments [18,19]. These studies have established that the first excited state, A $^2\Sigma^+$, decays by predissociation and fluorescence, and the B $^2\Pi$ and C $^2\Sigma^+$ states are completely predissociated; the results

* Corresponding author. E-mail: eland@physchem.ox.ac.uk

Dedicated to Professor Michael T. Bowers on the occasion of his 60th birthday.


*PII* S1387-3806(98)14181-7

include many details of the low energy dissociation processes, particularly those from the $A\ ^2\Sigma^+$ state and in the Franck–Condon gap between the ground state and the A state [17]. Because of limited mass resolution, the most complete TPEPICO study of dissociation from the outer valence states [17] did not distinguish between $N_2^+$ and $NO^+$, though this problem was overcome in later incompletely published work [16,20]. All previous coincidence measurements have been confined to the HeI region.

In this article we report PEPICO experiments covering the whole valence ionisation spectrum of $N_2O$ up to 40 eV, with good mass resolution. Nitrous oxide is interesting for a new PEPICO study, because its linear asymmetric geometry could allow anisotropy in the direction of fragment ions relative to the ejected electrons to manifest itself as forward/backward asymmetry of the time-of-flight (TOF) peaks. Such electron–ion angular correlations have recently been found in PEPICO work on inner valence ionisation of diatomic molecules [21,22], but no case is yet known in a linear triatomic species. Dissociation faster than molecular rotation is necessary for observation of a strong effect, and this condition might be expected to prevail for some of the higher energy ionisation bands of $N_2O$.

Nitrous oxide is a significant minor constituent of the Earth's atmosphere. The ion $N_2O^+$ may occur as a transient intermediate in ion–molecule reactions in the ionospheres of Earth, Mars, and Venus [23]; if these reactions do involve a triatomic ion intermediate, the unimolecular dissociative ionisation behaviour of $N_2O$ may cast light on the outcomes of the atmospheric bimolecular processes. The ionospheric reaction $O^+ + N_2 \rightarrow NO^+ + N$ involves the lowest quartet state surface, and has been discussed in detail in earlier work [11,16,19]. In this paper we consider whether some excited state reactions on doublet surfaces may be related to the observed dissociation behaviour of $N_2O^+$.

## 2. Experimental methods

The improved PEPICO apparatus has been described in detail elsewhere [24]. Briefly, ionisation occurs where wavelength-selected light from an atomic discharge lamp meets an effusive jet of target gas in the ionisation source. Electrons are energy analysed in a hemispherical condenser fitted with a position-sensitive detector; when an electron is detected a drawout field of 200 V $cm^{-1}$ is applied as a pulse to send ions through a two-field time-of-flight mass spectrometer to a multichannel plate detector. The mass resolution for thermal ions is about 200. The electron energy resolution is set by the choice of pass energy; it is 50 meV for 5 eV pass, used for the highest resolution scans, and 300 meV at 30 eV pass as used for most scans in the inner valence region. The photoelectron spectra were calibrated using the known energies of the $N_2O$ ionic states.

Mass spectra detected in coincidence with each photoelectron energy give the relative intensities of the competing product ions as peak areas. Each peak shape in such a mass spectrum represents a combination of the kinetic energy release distribution (KERD) in the reaction forming the ion, with the ion angular distribution. The two contributions cannot generally be separated, so it is usually assumed that the angular distributions are isotropic. Where the dissociation reaction is slower than molecular rotation, this assumption is reasonable, because in the limit of many rotation periods only a small fraction of any initial anisotropy remains. If dissociation is faster than molecular rotation, the observable peak shape in electron–ion coincidence is an inextricable mixture of effects of the KERD, the fixed frame angular distribution and any correlation between them. Although the contributions cannot be separated, the phenomenon of fast dissociation can often be recognised by the existence of forward/backward asymmetry of the peak shapes. This is because whatever the true fixed-molecule angular distribution, all terms which produce forward/backward asymmetry vanish completely in the limit of many rotations [21]. In the current work, peak shapes have been surveyed for such asymmetry by using the classical parameter of skewness [25], or, where the position of the peak centre is already known, by using a ratio of intensities in the forward and backward halves of the peak. Cases where the parameters significantly exceed their uncer-

tainty have been examined individually and are reported below. The well-known apparatus effects on peak symmetry have been tested for by simulation; they are generally negligible for the kinetic energy releases encountered here and always favour the forward part over the backward part. The cases where we believe asymmetry exists in $N_2O$ dissociative ionisation happen to be in the opposite sense, the backward parts of the peaks being stronger.

To derive kinetic energy release distributions from peak shapes we have used a direct numerical inversion procedure which is equivalent to smoothing the peak, deconvoluting it, differentiating it, and applying a Jacobian to transform to an energy scale. The forward and backward halves of the peak are treated separately and give independent estimates of the kinetic energy release distribution; the difference between them gives a rough indication of the uncertainty. Besides the dubious assumption of isotropy, statistical noise on the peaks, the limited time resolution and uncertainty over the exact thermal motion contribution all limit the accuracy of the resulting KERDs. The inversion parameters are set by manual adjustment to extract the least structured KERD consistent with the raw data. Although the resulting KERDs are of low energy resolution, they differ significantly from one ion and energy to another, as illustrated by two representative examples shown in Fig. 1. The KERDs are described in words in the following sections; each report is a distillation of the common factors from analyses of at least two separate experiments.

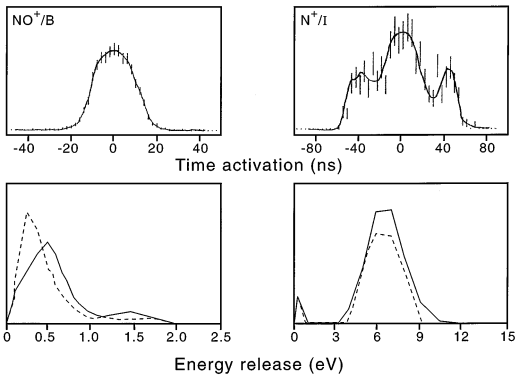


Fig. 1. Illustration of the derivation of kinetic energy release distributions (KERDs) from time-of-flight peak shapes. The error bars in the upper panels are the raw data for $NO^+$ from $N_2O^+$(B) at 18.25 eV, and for $N^+$ from $N_2O^+$ formed at 37–39 eV in the band later designated as I. The continuous lines in the upper panels show the fit to the data. Separate KERDs for forward (full line) and backward (dashed line) flying ions are shown in the lower panels.

## 3. Results

An overview of the behaviour of $N_2O^+$ is given in Fig. 2 as a low resolution scan of photoelectron spectra coincident with different product ions under HeII excitation, and in Fig. 3 as mass spectra coincident with electrons of different energies. The dissociation limits for fragmentation of $N_2O^+$ are summarised in Table 1 together with the ionisation energies for formation of its known electronic states for comparison with the experimental results. Vibrationally resolved branching to different final products from the A, B, and C states is illustrated in Figs. 4–7, and is summarised in Table 2 together with data on the higher states. Fig. 8 shows coincident photoelectron spectra in the inner valence region. Details of each reaction are given in the following paragraphs.

### 3.1. Ground state of $N_2O^+$, $X\,^2\Pi$

All vibrational levels of the ground state populated by direct photoionisation are below the first dissoci-

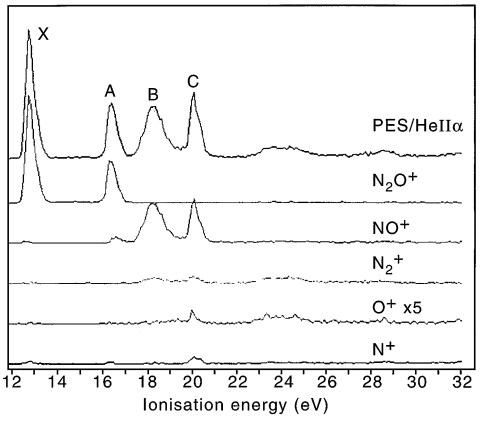


Fig. 2. Overall photoelectron spectrum and photoelectron spectra coincident with each product ion over the main part of the valence ionisation range, excited by HeII light (30.4 nm).

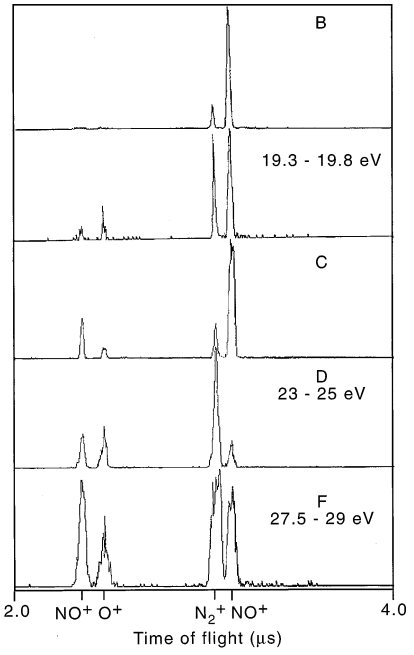


Fig. 3. Mass spectra coincident with photoelectrons in the designated bands under HeII excitation.

ation limit of 14.18 eV. Vibrational levels above this limit can be populated by autoionisation at specific wavelengths and are observed in variable-wavelength

Table 1
Dissociation limits and ionisation limits for $N_2O^+$

| | eV | Products of fragmentation |
|---|---|---|
| | **12.89** | X $^2\Pi$ |
| 1 | 14.19 | $NO^+(X\ ^1\Sigma^+) + N(^4S_u)$ |
| 2 | 15.29 | $N_2(X\ ^1\Sigma_g^+) + O^+(^4S_u)$ |
| | **16.38** | A $^2\Sigma^+$ |
| 3 | 16.57 | $NO^+(X\ ^1\Sigma^+) + N(^2D_u)$ |
| 4 | 17.25 | $N_2^+(X\ ^2\Sigma_g^+) + O(^3P_g)$ |
| | **17.65** | B $^2\Pi$ |
| 5 | 17.77 | $NO^+(X\ ^1\Sigma^+) + N(^2P_u)$ |
| 6 | 18.39 | $N_2^+(A\ ^2\Pi_u) + O(^3P_g)$ |
| 7 | 18.61 | $N_2(X\ ^1\Sigma_g^+) + O^+(^2D_u)$ |
| 8 | 19.22 | $N_2^+(X\ ^2\Sigma_g^+) + O(^1D_g)$ |
| 9 | 19.46 | $NO(X\ ^2\Pi) + N^+(^3P_g)$ |
| | **20.11** | C $^2\Sigma^+$ |
| 10 | 20.31 | $N_2(X\ ^1\Sigma_g^+) + O^+(^2P_u)$ |
| 11 | 20.34 | $N_2^+(A\ ^2\Pi_u) + O(^1D_g)$ |
| 12 | 20.48 | $N_2^+(B\ ^2\Sigma_u^+) + O(^3P_g)$ |
| 13 | 20.6 | $NO^+(a\ ^3\Sigma^+) + N(^4S_u)$ |
| 14 | 21.36 | $NO(X\ ^2\Pi) + N^+(^1D_g)$ |

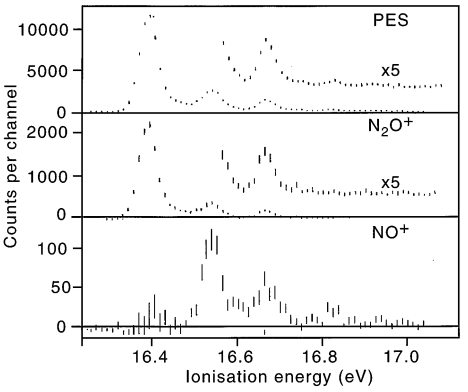


Fig. 4. Photoelectron spectrum and coincident photoelectron spectra for the A $^2\Sigma^+$ state of $N_2O^+$ with HeI excitation and 50 meV resolution.

photoelectron spectroscopy [15,26,27]. Within the "Franck–Condon gap" the molecular ions fragment to $NO^+$ from levels below the $O^+$ threshold (Table 1), but mainly to $O^+$ from higher levels [26].

### 3.2. $N_2O^+$ A $^2\Sigma^+$

The (000) level of the *A* state at 16.38 eV is above the first two dissociation limits; a third limit is within the energy range of the band. Dissociation from this state goes to $NO^+$ only; it has been very extensively studied by a variety of methods [11–17,25–27]; the (000) level fluoresces to the ground state X $^2\Pi$ to produce stable $N_2O^+$ ions, whereas fluorescence and predissociation compete as decay processes for the higher vibrational levels, whose lifetimes are known and much longer than rotation times [28–30]. The fluorescence quantum yield [28,29] is unity for A $^2\Sigma^+$(000) and smaller for the excited levels. The branching ratios from our data (Fig. 4, Table 2) agree satisfactorily with the fluorescence yields and previous PEPICO and TPEPICO work (Table 3). Kinetic energy releases derived on the assumption of isotropic angular distributions agree well with the results of Richard–Viard et al. [16,20], but are less detailed because of the higher drawout field used in the present experiments. For the (100) level, for example, the measured KERs of 1.8, 1.5, 1.2, and 1 eV correspond to the formation of $NO^+(X\ ^1\Sigma^+) + N(^4S_u)$ with

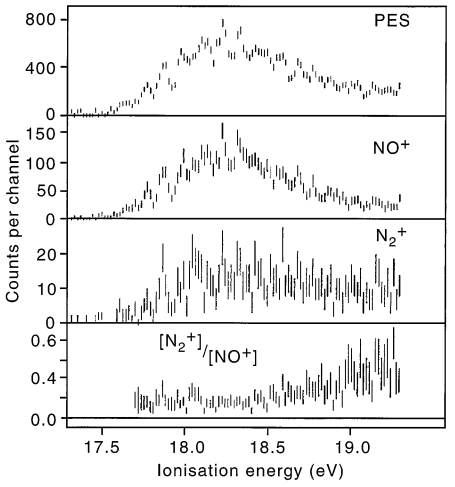


Fig. 5. Photoelectron spectrum and coincident photoelectron spectra for the B $^2\Pi$ state of $N_2O^+$ with HeI excitation and 50 meV resolution. The bottom panel shows the intensity ratio of $N_2^+$ to $NO^+$.

maximum population at $v = 4$ in the $NO^+$ ion, in good agreement with previous TPEPICO and FIBLAS results. Dissociation from the (101) level produces maximum population of $NO^+$ $v = 5$. As expected from the long lifetimes before dissociation, the $NO^+$ peak shapes in dissociation from this state are forward/backward symmetric under both HeI and HeII ionisation.

### 3.3. $N_2O^+$ $B\ ^2\Pi$

The B state band of the $N_2O^+$ spectrum has a complex vibrational structure with narrow linewidths; the band is only partially resolved in this experiment (Fig. 5). At the onset of the band, four product channels are energetically accessible; several more channels open within the band. Although the fragments $NO^+$, $N_2^+$, and $O^+$ could all be formed, the coincidence spectra show negligible $O^+$ intensity in the main part of the band; the major product from all the $N_2O^+$(B) vibrational levels is $NO^+$, with $N_2^+$ formed in smaller abundance. The proportions of $NO^+$ and $N_2^+$ remain essentially constant at about 5:1 over the low energy and central part of the band, but at higher energy the proportion of $N_2^+$ gradually increases (Fig. 5). There are no sudden changes at energies where new product channels open. In the energy range 19 to 20 eV, above B and just below the C state, there is significant production of $O^+$ and $N^+$ in addition to $NO^+$ and $N_2^+$ (Fig. 3). This is the energy region where Potts and Williams [4] detected a low intensity configuration interaction (CI) band, and where some theoretical calculations suggest the existence of a $^4\Pi$ state [31,32]. Other earlier calculations suggested the possible existence of several extra states including $^2\Pi$ states in the same energy region [33,34]. The substantial change in branching ratios, different in this range from those at both higher and lower energy, supports the idea that a distinct electronic state may be present.

The kinetic energy releases in dissociations from the B state have not been studied systematically before. In both $NO^+$ and $N_2^+$ formation the kinetic energy release distributions are broad, and the average energy releases increase much less rapidly than the available energy as the band is traversed. At the onset of the band, at a mean ionisation energy of 17.8 eV, $NO^+$ is formed with a most probable energy release of 0.6 eV and a maximum of 1 eV. This distribution strongly suggests that the products formed are entirely $NO^+(X\ ^1\Sigma^+) + N(^2D_u)$, the $NO^+$ being vibrationally excited to a range of levels, mainly to $v = 3$. At the peak of the band, at an energy of 18.25 eV, the most probable energy release is about 0.5 eV, and the maximum is about 1.5 eV (Fig. 1). This shows that the products are highly excited, possibly vibrationally but more likely with formation of $NO^+(X\ ^1\Sigma^+) + N(^2P_u)$. This is clearer at higher energies in the band, where the $NO^+$ KERD becomes more strongly bimodal, suggesting that the products are formed at both doublet limits; the lower kinetic energy release is always favoured over the higher one. At energies just below the C state, 19.5–20 eV, the KERD is certainly bimodal and possibly trimodal, with a maximum energy release of about 2 eV with significant intensity.

For the $N_2^+$ ion the KER at the onset of the *B* band is about 0.2 eV, compared with an available energy of 0.5 eV for formation of ground state products. This shows that the $N_2^+$ is mildly vibrationally excited. At

the centre of B, 18.25 eV, the main KER is 0.4 eV with a maximum of 0.8 eV ($E_{av1}$ = 1 eV), showing stronger vibrational excitation. The KERD hardly changes at higher energies within B and in the range up to 20 eV; it seems likely that the products are formed in excited electronic as well as vibrational states when the two new channels become open (Table 1). Formation of $N_2^+(A\ ^2\Pi_u)$ would be consistent with the observation of fluorescence emission with a microsecond lifetime in coincidence with this ion in photoionisation of $N_2O$ [35]. However, the known lifetime [34] of $N_2^+(A\ ^2\Pi_u)$ is longer than the one measured in the coincidence experiment [35], and this emission has not been identified in either flowing afterglows [34] or electron impact excitation [36] of $N_2O$.

The peaks for both $NO^+$ and $N_2^+$ are forward/backward symmetric, at all energies within the B band; their shapes are the same under HeI and HeII excitation.

### 3.4. $N_2O^+$ $C\ ^2\Sigma^+$

The vibrational structure of the C $^2\Sigma^+$ band is dominated by the (000) level, but at high resolution it also shows excitation of all three vibration modes [2,37,38]; there is no detectable line broadening. Only the (100) and (001) levels are resolved in the present experiment (Fig. 6). A product channel for $N^+$ formation opens below the C state at 19.46 eV, so dissociation from this state can produce the four ion fragments $NO^+$, $N_2^+$, $O^+$, and $N^+$. For all three vibrational levels the main ion fragment produced is $NO^+$, with $N_2^+$ and $N^+$ competing as the next largest fraction (Table 2); $O^+$ is produced to a small extent. The pattern of branching to different products is the same on the (000) and (100) levels, but the (001) level dissociates more strongly to $N^+$ and less to $N_2^+$ than the other levels (Fig. 7).

The $NO^+$ fragment ions from C $^2\Sigma^+(000)$ have a wide kinetic energy release distribution peaking at around 1 eV which can be interpreted as formation of $NO^+(X\ ^1\Sigma^+) + N(^2P_u)$ with $NO^+$ in the vibrational states $v$ = 0–6. The KERDs from (100) and (001) are not distinguishably different. Under HeI (58.4 nm) excitation, the TOF peaks from all three levels are forward/backward symmetric.

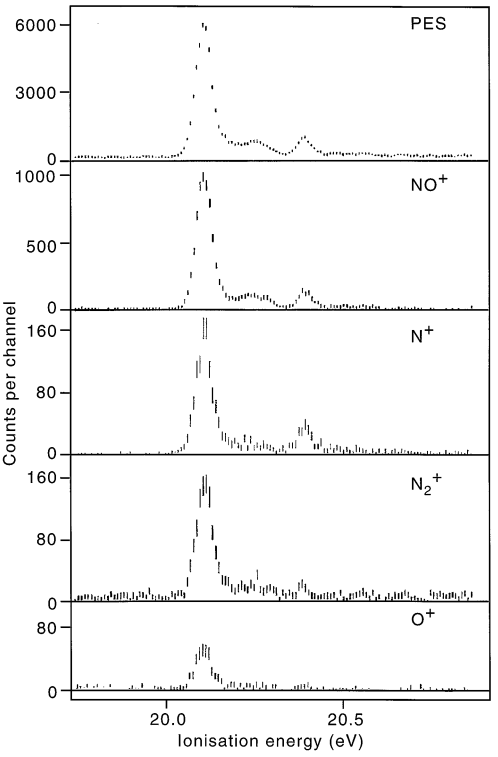


Fig. 6. Photoelectron spectrum and coincident photoelectron spectra for the C $^2\Sigma^+$ state of $N_2O^+$ with HeI excitation and 50 meV resolution.

The $N_2^+$ ions from C $^2\Sigma^+(000)$ have a bimodal KERD which suggests that $N_2^+$ is formed partly as $N_2^+(A\ ^2\Pi_u) + O(^3P_g)$ and partly as $N_2^+(X\ ^2\Sigma_u) + O(^1D_g)$. Higher resolution kinetic energy measurements will be needed to clarify this.

For the $N^+$ fragment ion, the KER in formation from C $^2\Sigma^+(000)$ peaks at 0.25 eV and has a maximum at about 0.4 eV. As the available energy is just 0.65 eV, this shows that the neutral NO fragment is formed mainly in vibrationally excited levels $v$ = 1 and $v$ = 2. The KER is visibly higher in formation from (001), but of the same form.

The $O^+$ ion has a most probable KER of about 0.6 eV when formed from C $^2\Sigma^+(000)$. This low kinetic energy suggests that it is formed as $O^+(^2D_g)$ with ground state $N_2$ in a range of low vibrational levels.

Table 2
Branching ratios in $N_2O^+$ dissociation

| | $N_2O^+$ | $NO^+$ | $N_2^+$ | $O^+$ | $N^+$ |
|---|---|---|---|---|---|
| A state | | | | | |
| 0,0,0 | 100% | 0 ± 4% | ... | ... | ... |
| 1,0,0 | 75 ± 2% | 24 ± 5% | 0 ± 4% | 0 ± 4% | 0 ± 4% |
| 0,0,1 | 72 ± 2% | 21 ± 5% | 0 ± 6% | 1 ± 6% | 0 ± 6% |
| 1,0,1 | 36 ± 11% | 40 ± 11% | 5 ± 6% | 1 ± 6% | 1 ± 6% |
| B state region | | | | | |
| 17.7–18.9 eV | 1 ± 12% | 86 ± 3% | 13 ± 3% | 3 ± 11% | −2 ± 12% |
| 19–19.9 eV | —[a] | 62 ± 3% | 29 ± 3% | 7 ± 1% | 2 ± 1% |
| C state | | | | | |
| 0,0,0 | 0 ± 2% | 74 ± 1% | 10 ± 2% | 4 ± 2% | 12 ± 2% |
| 1,0,0 | 2 ± 4% | 70 ± 1% | 16 ± 3% | 3 ± 4% | 9 ± 4% |
| 0,0,1 | 1 ± 5% | 69 ± 1% | 9 ± 4% | 3 ± 5% | 18 ± 4% |
| Inner valence region | | | | | |
| D, 22–26 eV | 3 ± 7% | 10 ± 7% | 59 ± 3% | 16 ± 6% | 12 ± 6% |
| E, 26–27.5 eV | 3 ± 19% | 13 ± 17% | 41 ± 12% | 18 ± 16% | 26 ± 15% |
| F, 28–30 eV | 2 ± 16% | 23 ± 12% | 36 ± 10% | 17 ± 10% | 23 ± 12% |
| G, 31–34.5 eV | —[a] | 22 ± 5% | 19 ± 2% | 12 ± 1% | 47 ± 5% |
| H, 34.5–37 eV | —[a] | 34 ± 5% | 12 ± 2% | 9 ± 1% | 45 ± 5% |
| I, 38–40.5 eV | —[a] | 46 ± 8% | 16 ± 3% | 11 ± 2% | 27 ± 5% |

[a] In regions of weak signal and low electron energy, scattered high energy electrons give an unquantifiable false parent ion signal.

There are too few counts to determine the KERD from higher levels of C.

When HeII (30.4 nm) ionisation is used, the different vibrational levels in C are not resolved. The overall peak shapes for all ion products are almost the same as observed by using HeI and selecting C $^2\Sigma^+(000)$.

### 3.5. The HeII region

The HeII region contains several broad features. No vibrational fine structure is known and there is definitely none in the bands up to 28 eV in the high resolution (10 meV or better) spectrum taken recently at Uppsala [38]. The positions of the bands in our spectrum (Fig. 8) agree with the band positions found by Holland et al. [8] in spectra at different wavelengths. For convenience of reference, we have marked six bands in Fig. 8 with alphabetical labels, continuing the sequence of the inner valence bands. The main feature of the dissociation branching in this region is that $N_2^+$ rather than $NO^+$ is the dominant fragment. The relative intensities of the four different ionic fragments are similar for the bands up to 31 eV,

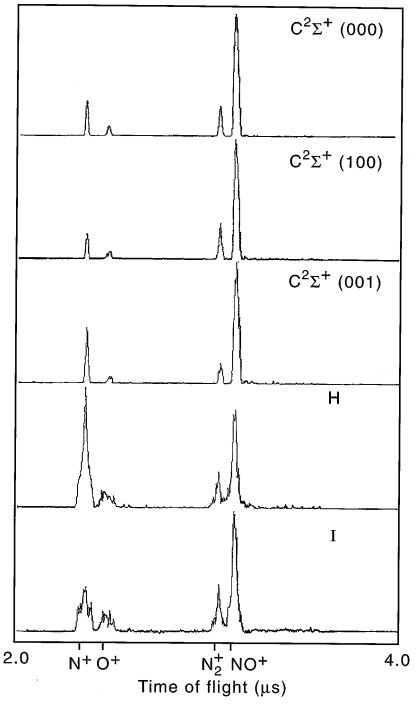


Fig. 7. Mass spectra coincident with the resolved vibrational levels of $N_2O^+(C\ ^2\Sigma^+)$ and with electrons from the two highest energy bands in the HeII spectrum.

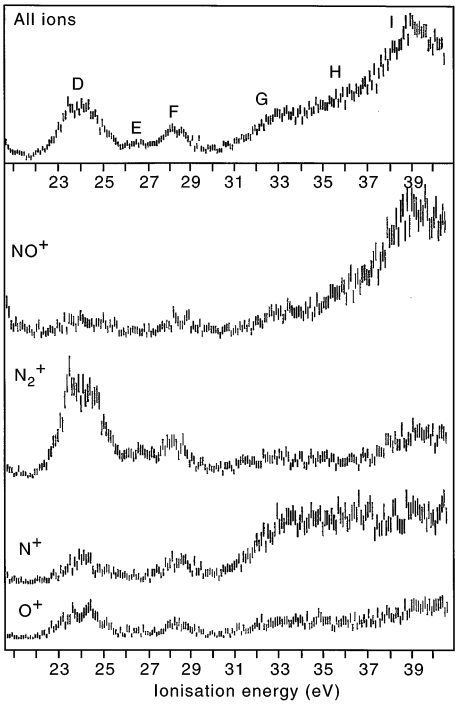


Fig. 8. Photoelectron spectrum and coincident photoelectron spectrum in the inner valence region, excited by HeII (30.4 nm) radiation.

except that band D (at 24 eV) dissociates with a strong preference towards $N_2^+$ (Fig. 8, Table 2). The form of the spectra between 31 and 40 eV is similar in the $N_2^+$ and $O^+$ channels where the N–O bond is broken, but different from the form in the $NO^+$ and $N^+$ channels where the bond broken is N–N.

The continuous form of the inner valence bands, which may arise from fast dissociation, inspired a careful search of the TOF peak shapes for forward/backward asymmetry. An unmistakable effect is found only for the $N_2^+$ fragment from bands E and F, in the energy range 26–30 eV; it is shown in Fig. 9. The $N_2^+$ peak shapes in this range show that $N_2^+$ and the photoelectron are ejected preferentially in the same direction, that is, into the same hemisphere centred on the original molecule. Because of the possibly anisotropic distributions and the rather few counts recorded, the KERDS deduced from peak shapes in this energy region must be interpreted with caution. The results for bands D to I are summarised

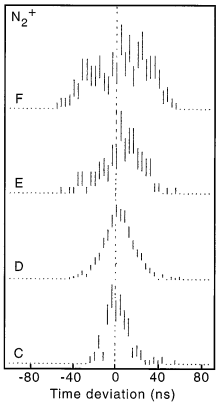


Fig. 9. Time-of-flight peak shapes for $N_2^+$ from the different $N_2O^+$ bands designated C–F, showing the forward/backward asymmetry of two of the peaks. The skewness parameters for the bands C–F are $-0.15 \pm 0.15$, $-0.06 \pm 0.07$, $0.72 \pm 0.17$, and $0.35 \pm 0.13$, confirming what is apparent to the eye. The same result that there is distinct forward/backward asymmetry in $N_2^+$ formation from bands E and E has been obtained in three separate runs.

in Table 3, which presents several points of interest. In $NO^+$ formation the main energy releases from the D, E, F, and G states are low, showing that products with very high internal energies are formed. For $N_2^+$, by contrast, the energy releases from states D, E, F, and G are higher and rise in step with the ionisation energy, suggesting that the same set of products is reached from all the initial states. There are several possible candidates at energies around 21 eV, and we cannot decide definitely which is reached on the basis of the kinetic energy release alone. The rather intense emission from $N_2^+(B\ ^2\Sigma_u^+)$ in electron impact [36] and flowing afterglows [34] with $N_2O$ suggests, however, that the products may be $N_2^+(B\ ^2\Sigma_u^+) + O(^3P_g)$ at 20.48 eV. For $N^+$, the peaks are triangular when the ion is formed from states F and G, showing that the KERDs are very broad. From H and I very clear bimodal distributions are found for $NO^+$ and $N^+$, as can be seen directly in the peak shapes (Figs. 1 and 7); despite the quite high energy releases, very highly excited products are formed. In $O^+$ formation from G, H, and I the energy release is very large, around 10 eV. The peak shapes are apparently asymmetric when $O^+$ is formed from H and I, in the sense that the electron and ion tend to go in opposite directions.

Table 3
Kinetic energy release distributions in the inner valence region

| | Energy range | $NO^+$ | $N^+$ | $N_2^+$ | $O^+$ |
|---|---|---|---|---|---|
| D | 21.9–25.8 eV | Bimodal<br>0.4 eV<br>2.3 eV | Bimodal<br>0.2 eV<br>2.1 eV | Broad KERD from 0.1 to 3 eV | Bimodal(?) 0.65 eV 3 eV |
| E | 25.8–27.3 eV | Bimodal<br>0.2 eV<br>1.7 eV | (Too weak) | Asymmetric single KER (?) 5.8 eV | (Too weak) |
| F | 27.3–29.8 eV | 1.7 eV | Broad 0 to 4 eV | Asymmetric single KER 6.6 eV | (Too weak) |
| G | 32–35 eV | Wide spread 0–4 eV | Broad 0 to 5.3 eV | Single KER 13 eV | Single KER(?) 10 eV |
| H | 35–37 eV | Bimodal<br>0.65 eV<br>7.0 eV | Bimodal<br>0.35 eV<br>7.5 eV | (Overlaps too much) | Possibly asymmetric ~10 eV |
| I | 37–40 eV | Bimodal<br>1.0 eV<br>8.8 eV | Bimodal<br>0.85 eV<br>7.8 eV | Bimodal<br>0.4 eV<br>7 eV | Possibly asymmetric ~10 eV |

Because the energy release is so large, however, we cannot rule out an apparatus effect in this case.

## 4. Discussion

The dissociations of $N_2O^+$ seem to divide into two regions; in the realm of the single-hole outer valence states the major product is $NO^+$, whereas in the inner valence region it is $N_2^+$ that dominates. Even the unidentified interloper "quasistate" [39,40] between B and C shares the characteristic of higher $N_2^+$ production with the inner valence states. If this trend is more than chance, it might be related to the increase in N(2s) atomic orbital character at the higher energies. In the outer valence region, the dissociation of the A state of $N_2O^+$ has been discussed in detail before [15–20] on the basis of theoretical potential energy surfaces calculated by Hopper [31] and Komiha [32] and theoretical models [41]. The A state ions can decay only to products on a quartet surface; for all the higher $N_2O^+$ states doublet dissociation channels are energetically accessible and we believe they predominate. These higher state dissociations have been discussed in terms of an adiabatic correlation diagram for linear ions [20], reproduced with slight modification in Fig. 8. However, there is a possibility, hinted at by the odd-quantal excitation of the bending vibration in the C-state band [2,36,38], that bent forms of the molecular ion may also be involved. The C state is the first one to correlate directly to $N^+$ and $O^+$, perhaps explaining why these two products are not formed from the lower states even where it would be possible energetically and is allowed by the spin rule.

Dissociation must be faster than rotation in dissociation of the inner valence states forming bands E and F where the $N_2^+$ peak is asymmetric; the lack of fine structure in the photoelectron spectrum leaves open the possibility of decay within a vibrational period. The lack of detectable forward/backward asymmetry for other ionic products from the same bands is disappointing, because any competing decays from the same states would also have to be fast and would share the same electron ejection anisotropy. One possibility is that the broad photoelectron bands include several states; better data will be required to clarify this.

The branching to final products from all the valence states of $N_2O^+$ is distinctive, and demonstrates the state-specific behaviour expected in a triatomic. The change in branching in the zone between B and C, which supports the existence of a new electronic state in this region, demonstrates this clearly. The behaviour of the inner valence states in dissociation also varies as a function of the ionisation energy, but does not show specific changes from one band to the next. This smoothly varying branching behaviour has

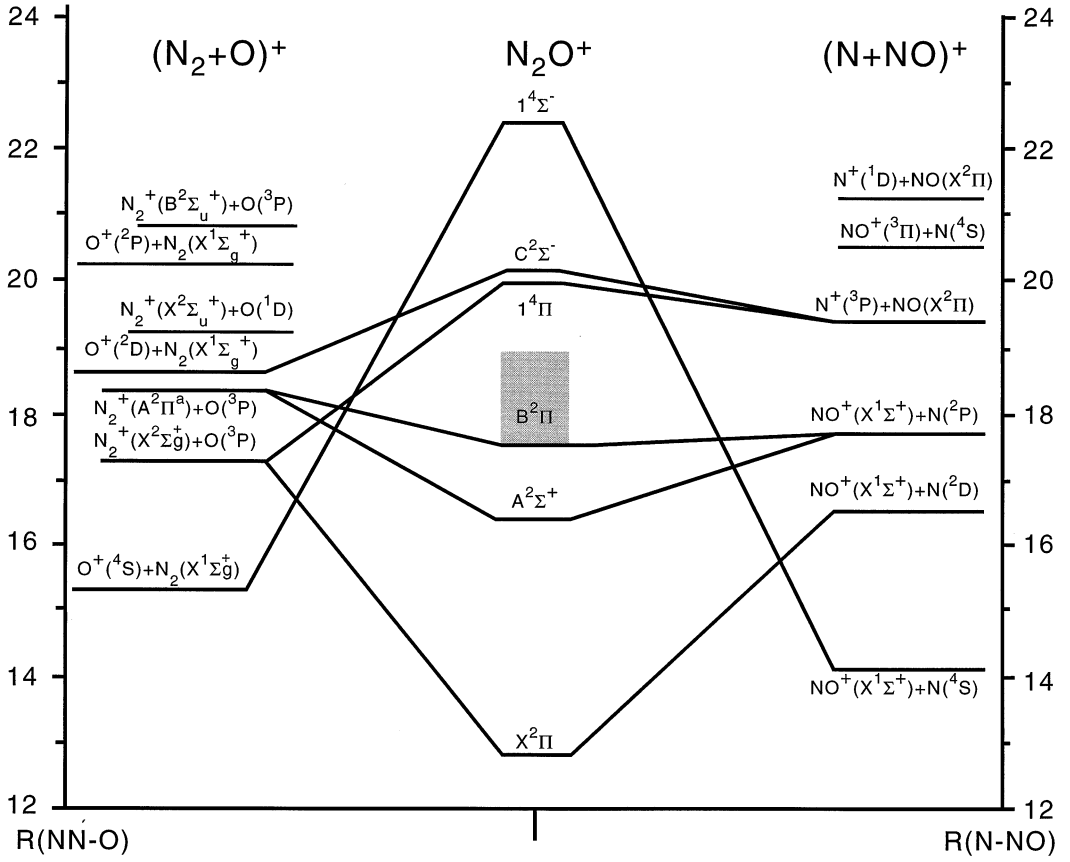


Fig. 10. Adiabatic correlation diagram for $N_2O^+$ following Richard-Viard [20].

been noted before in inner valence regions, particularly for CO [22].

The reaction of $O^+(^2P_u)$ with $N_2$, whose asymptotic energy is very close to the C $^2\Sigma^+$ state of $N_2O^+$, is the major loss process for excited oxygen ions in the terrestrial dayside ionosphere [23]. The reaction has been studied over a range of centre-of-mass collision energies by Lavollee and Henri [42], and most recently by Li and collaborators [43]. The main reaction channels are charge exchange (to $N_2^+$) and quenching, but with some $NO^+$ production in reactive scattering. Li et al. [43] showed that in contrast to the behaviour of $O^+(^2D)$, the cross section for formation of $NO^+$ by reaction of $O^+(^2P)$ with $N_2$ is highest at the lowest collision energy. This certainly leaves open the possibility that $N_2O^+$(C) is formed as an intermediate. The yield of $N^+$, though small and rising towards higher collision energies, also is consistent with this hypothesis, following the present branching ratio from $N_2O^+$(C).

## 5. Conclusions

The nitrous oxide ion still holds many mysteries, despite years of work on its spectrum and dissociations. It seems that the strong one-electron ionisation bands in its photoelectron spectrum may conceal “dark” states, whose presence can be revealed through their dissociation behaviour. The associations found here between dissociation pathways and both electronic states and vibrational levels directly demonstrate that a statistical model of the dissociation process is not appropriate. Against this, dissociation

behaviour changes very smoothly with energy in the inner valence region, although theoretical models predict the existence of many states there, perhaps suggesting that the states are strongly coupled. A detailed understanding of the passage from molecular ions of selected internal energy in particular states and levels to final states of the products must await more theoretical progress.

## References


[1] C.R. Brundle, D.W. Turner, Int. J. Mass. Spectrom. Ion Phys. 2 (1969) 195.
[2] P.M. Dehmer, J.L. Dehmer, W.A. Chupka, J. Chem. Phys. 73 (1980) 126.
[3] K. Kimura, S. Katsumata, Y. Achiba, T. Yamazaki, S. Iwata, "Handbook of HeI Photoelectron Spectra of Fundamental Organic Molecules", Halsted, New York, 1981.
[4] A.W. Potts, T.A. Williams, J. Electron Spectrosc. Relat. Phenom. 3 (1974) 3.
[5] W. Domcke, L.S. Cederbaum, J. Schirmer, W. von Niessen, C.E. Brion, K.H. Tan, Chem. Phys. 40 (1979) 171.
[6] H. Nakatsuji, Chem. Phys. 75 (1983) 425.
[7] U. Gelius, J. Electron Spectrosc. Relat. Phenom. 5 (1974) 985.
[8] D.M.P. Holland, M.A. MacDonald, M.A. Hayes, Chem. Phys. 142 (1990) 291.
[9] R. Fantoni, A. Guardini-Guidoni, R. Tiribelli, R. Camilloni, G. Stefani, Chem. Phys. Lett. 71 (1980) 335.
[10] A. Minchinton, I. Fuss, E. Weigold, J. Electron Spectrosc. Relat. Phenom. 27 (1982) 1.
[11] J. Berkowitz, J.H.D. Eland, J. Chem. Phys. 67 (1977) 2740.
[12] T. Masuoka, S. Mitani, J. Chem. Phys. 90 (1989) 5.
[13] J.H.D. Eland, Int. J. Mass Spectrom. Ion Phys. 12 (1973) 389.
[14] B. Brehm, R. Frey, A. Kustler, J.H.D. Eland, Int. J. Mass. Spectrom. Ion Phys. 13 (1974) 251.
[15] T. Baer, P.-M. Guyon, I. Nenner, A. Tabché-Fouhaillé, R. Botter, L.F.A. Ferreira, T.R. Govers, J. Chem. Phys. 70 (1979) 1585.
[16] M. Richard-Viard, O. Atabek, O. Dutuit, P.-M. Guyon, J. Chem. Phys. 93 (1990) 12.
[17] I. Nenner, P.-M. Guyon, T. Baer, T.R. Govers, J. Chem. Phys. 72 (1980) 6587.
[18] S. Abed, M. Broyer, M. Carré, M.L. Gaillard, M. Larzillière, Phys. Rev. Lett. 49 (1982) 120.
[19] J. Lermé, S. Abed, M. Larzillière, R.A. Holt, M. Carré, J. Chem. Phys. 84 (1986) 2167.
[20] M. Richard-Viard, Thèse de Doctorat, Université Paris-Sud, Orsay, France, 1988.
[21] J.H.D. Eland, E.J. Duerr, Chem. Phys. 229 (1998) 1.
[22] J.H.D. Eland, E.J. Duerr, Chem. Phys. 229 (1998) 13.
[23] A. Dalgarno, J.L. Fox, In "Unimolecular and Bimolecular Ion Molecule Reaction Dynamics", C.Y. Ng, T. Baer, I. Powis (Eds.), Wiley, Chichester, 1994.
[24] T. Field, J.H.D. Eland, Meas. Sci. Technol. 9 (1998) 922.
[25] O.L. Davies, "Statistical Methods in Research and Development", Oliver and Boyd, London, 1947.
[26] M. Richard-Viard, A. Delboulbé, M. Verloet, Chem. Phys. 209 (1996) 159.
[27] E. Sokell, A.A. Wills, J. Comer, J. Phys. B 29 (1996) 3417; ibid, 30 (1997) 2635.
[28] R. Frey, B. Gotchev, W.B. Peatman, H. Pollak, E.W. Schlag, Chem. Phys. Lett. 54 (1978) 411.
[29] J.P. Maier, F. Thommen, Chem. Phys. 51 (1980) 319.
[30] D. Klapstein, J.P. Maier, Chem. Phys. Lett. 83 (1981) 590.
[31] D.G. Hopper, J. Am. Chem. Soc. 100 (1978) 109; J. Chem. Phys. 72 (1980) 3679.
[32] N. Komiha, Thesis, Université Pierre et Marie Curie, Paris, 1981; J. Mol. Struct. 306 (1994) 313.
[33] W.B. Maier, R.F. Holland, J. Chem. Phys. 59 (1973) 4515.
[34] M. Tsuji, K. Tsuji, Y. Nishimura, Int. J. Mass Spectrom. Ion Phys. 30 (1979) 175.
[35] T. Field, J.H.D. Eland, Chem. Phys. Lett. 197 (1992) 542.
[36] H.A. van Sprang, G.R. Möhlmann, F.J. de Heer, Chem. Phys. 33 (1978) 65.
[37] M.J. Weiss, Chem. Phys. Lett. 39 (1976) 250.
[38] L. Karlsson, P. Baltzer, B. Wannberg, E. Kinmond, J.H.D. Eland (unpublished).
[39] J.C. Lorquet, C. Cadet, Int. J. Mass Spectrom. Ion Phys. 7 (1971) 245.
[40] H. Köppel, L.S. Cederbaum, W. Domcke, Chem. Phys. 69 (1982) 175.
[41] S. Miret-Artès, G. Delgado-Barrio, O. Atabek, J.A. Beswick, Chem. Phys. Lett. 98 (1983) 554.
[42] M. Lavollée, G. Henri, J. Phys. B. 22 (1989) 2019.
[43] X. Li, Y.-L. Huang, G.D. Flesch, C.-Y. Ng, J. Chem. Phys. 106 (1997) 1373.